

**UBTF Tandem Duplications with Recurrent *FLT3* and *WT1* Co-mutations
Drive *HOX* Dysregulation and Epigenetic Rewiring in Acute Myeloid
Leukemia**

By

Morgan Lallo

Dr. David Beck, Dr. Iannis Aifantis

SUMMARY

Mutations of Upstream Binding Transcription Factor (*UBTF*) have only recently been recognized in leukemia, most notably recurrent exon 13 tandem duplications (*UBTF-TDs*), suggesting a gain-of-function mechanism that extends *UBTF* activity beyond its canonical ribosomal DNA targets. Leukemogenic activity arises through aberrant interaction between *KMT2A* and its cofactor menin, resulting in dysregulated *HOX* gene expression, maintenance of a stem-like progenitor state, and a blockade in differentiation with uncontrolled self-renewal. This relation is of interest as *UBTF-TD* co-localizes at key regulatory regions with *KMT2A* and menin, and have been shown to be promising therapeutic targets to menin inhibitors. The recent discovery of novel *UBTF* alterations in hematologic malignancies underscores the critical need to elucidate the functional consequences of these co-mutational interactions and is essential to developing more effective, context-specific therapeutic strategies. Here, we use multi-omic profiling to characterize molecular mechanisms of *UBTF-TD* and their modulation by co-occurring mutations frequently observed in AML (*FLT3*, *NPM1*, *WT1*).

INTRODUCTION

Acute myeloid leukemia (AML) is a genetically heterogeneous and clinically aggressive hematologic malignancy characterized by the clonal expansion of immature myeloid progenitors with impaired differentiation and self-renewal, resulting in the expansion of immature blasts and subsequent hematopoietic failure.^{1,2,3,4} Timely diagnosis is critical, where patients typically present with a constellation of features including immunosuppression, myelosuppression manifesting as life-threatening anaemia or thrombocytopenia, and leukocytosis, prompting concern for an underlying hematological malignancy.⁵

Aberrations across multiple molecular layers including signal transducers, chromatin modifiers, transcription factors and splicing factors perturb key pathways that govern hematopoietic fate, collectively shaping the diverse mutational landscape that drive leukemogenesis in adult AML.^{10,11,12} Commonly mutated genes include *RAS*, *WT1*, *DNMT3A*, *TET2*, *IDH1/2*, and *ERG*, with *NPM1*, *FLT3*, and *CEBP α* closely linked to treatment response and disease progression.^{6,10,11,12} Epigenetic dysregulation via mutations in DNA methyltransferases (*DNMT1*, *DMNT3A*, *DNMT3B*) and TET family methylcytosine dioxygenases additionally represent a major axis of leukemia transformation.^{13,14}

The interplay among these mutations and potential burden of co-mutation further complicates the pathogenesis of AML. *NPM1* mutations are often associated with favorable prognosis¹⁵, whereas *FLT3* and *CEBPA* mutations confer adverse risk and are frequently co-mutated with *WT1*.¹⁶⁻¹⁹ *WT1* is a transcription factor that contributes to oncogenic transformation through epigenetic remodeling at target loci.^{17,20} *WT1* mutations are a particular challenge in AML as they display functional heterogeneity, acting either as oncogenic drivers or tumor suppressors, though their precise mechanisms in promoting leukemogenesis remain incompletely understood.²¹⁻²⁵ Clonal architecture studies suggest that *WT1* frequently serves as a founder mutation that cooperated with later-arising lesions, such as *FLT3-ITD*, to accelerate disease progression, and co-mutational patterns with *NPM1-WT1* have been implicated in relapse.²⁶

Mutations of the upstream binding transcription factor (*UBTF*) have only recently been recognized in leukemia, most notably recurrent exon 13 tandem duplications (*UBTF-TDs*), suggesting a gain-of-function mechanism that extends *UBTF* activity beyond its canonical rDNA targets.²⁶ *UBTF* encodes a nucleolar protein essential for ribosomal RNA (rRNA) transcription and nucleolar organization with emerging roles across neurodevelopmental disorders and oncogenesis.²⁷⁻³⁶ *UBTF-TDs* have been characterized as a recurrent distinct molecular subtype of childhood AML and is associated with *HOX* gene dysregulation.^{4, 38-41}

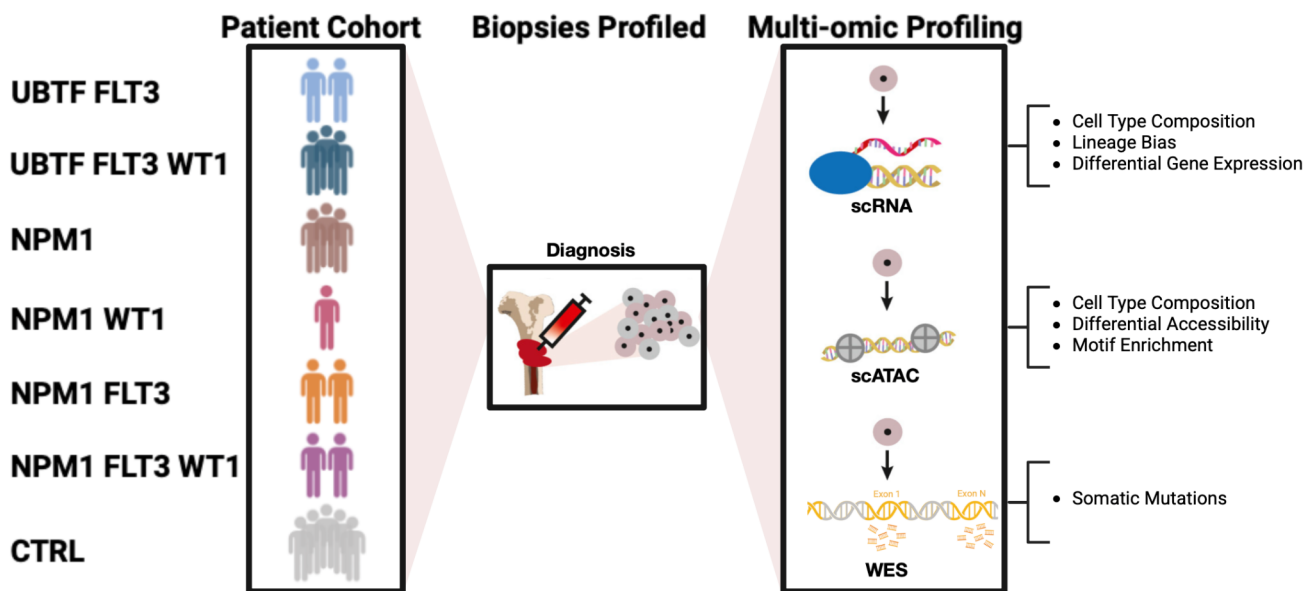
Recent findings reveal that *UBTF-TDs* extend beyond pediatric AML, a genetically distinct classification to adult AML,^{6,7,8,9} and occur in 3% of adult AML patients and are linked to elevated measurable residual disease (MRD) and poor prognosis.¹⁵ *UBTF-TDs* exhibit a distinct molecular profile from other AML subtype-defining alterations such as low bone marrow (BM) blast infiltration, high rates of *WT1*, *FLT3-ITDs*, and trisomy 8 mutations.²⁷ BM morphology commonly exhibits dysmyelopoiesis, though the extent of these abnormalities is shaped by the concurrent of *FLT3-ITD* mutations.²⁷ *UBTF-TD* AML patients have lower complete remission (CR) rates than *UBTF*-wild-type patients and an OS of 57.1% - statistically comparable to outcomes in intermediate and adverse-risk groups.²⁷ Analysis of paired diagnostic and relapsed/refractory samples revealed frequent clonal selection of *WT1*-mutant subpopulations following intensive chemotherapy, particularly in cases co-occurring with *UBTF-TD*, suggesting a role in treatment resistance to intensive chemotherapy (ICT) and disease recurrence.²⁷

The gain-of-function activity of *UBTF-TD* mutations mirrors that of other *HOX*-driven AML subtypes, such as *NPM1*-mutant and *KMT2A*-rearranged AML.^{38,42-44} Leukemogenic activity arises through aberrant interaction between *KMT2A* and its cofactor menin, resulting in dysregulated *HOX* gene expression, maintenance of a stem-like progenitor state, and a blockade in differentiation with uncontrolled self-renewal. Similarly, *UBTF-TD* AML transcriptionally resembles other *HOX*-high subtypes, particularly *NPM1*-mutant AML.³⁸ This relation is of interest as *UBTF-TD* co-localizes at key regulatory regions with *KMT2A* and menin, and have been shown to be promising therapeutic targets to menin inhibitors.³⁸ The recent discovery of novel *UBTF* alterations in hematologic malignancies underscores the critical need to elucidate the functional consequences of these co-mutational interactions and is essential to developing more effective, context-specific therapeutic strategies.

Here, we use multi-omic profiling to characterize molecular mechanisms of *UBTF-TD* and their modulation by co-occurring mutations frequently observed in AML (*FLT3*, *NPM1*, *WT1*). Our findings reveal that *UBTF-TD* *FLT3* mutations establish a robust stem-like transcriptional program marked by impaired differentiation and sustained progenitor identity. Notably, *UBTF-FLT3* double-mutant AMLs converge on a transcriptional bottleneck characterized by early myeloid progenitor expansion, *HOX*-driven self-renewal, and a failure to achieve terminal differentiation. Rather than multilineage priming, this state reflects arrested myeloid-biased stemness—further intensified by *WT1* co-mutation, which rewrites the epigenetic landscape through dysregulation of chromatin regulators such as *KAT6B*, *PRDM16*, and *DNMT3A*. This *UBTF*-specific transcriptional identity is parallel to that of *NPM1-FLT3* AMLs and may underlie the aggressive clinical phenotype associated with *UBTF*-mutant disease.

RESULTS

A



B

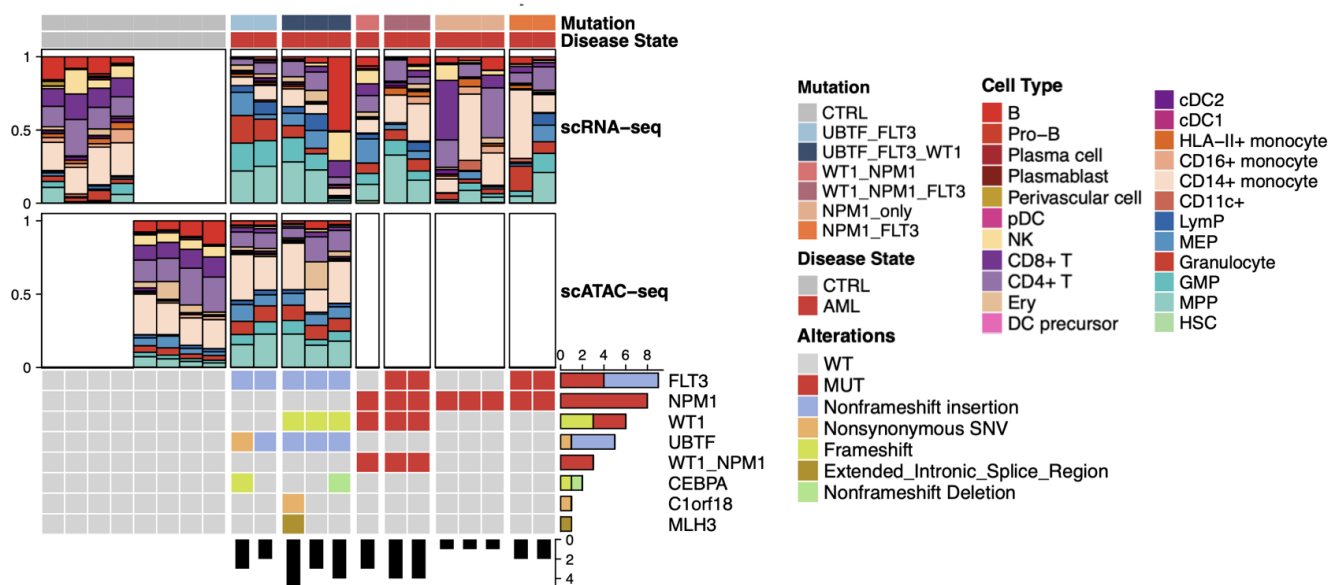


Figure 1. Integrated mutational and cellular landscape of the AML cohort

(A) Overview of the multi-omic profiling strategy used to characterize AML samples. Single-cell RNA-seq (scRNA-seq) and single-cell ATAC-seq (scATAC-seq) were performed to assess cell type composition, gene expression, chromatin accessibility, and transcription factor (TF) activity. Whole exome sequencing (WES) was used to identify somatic and recurrent co-mutations. (B) Stacked bar plots represent the proportional abundance of annotated cell types in scRNA-seq (top) and scATAC-seq (middle) data across the entire cohort. Somatic mutations identified from WES (bottom) are annotated per patient sample. Matched multi-omic data for individual patients are aligned vertically.

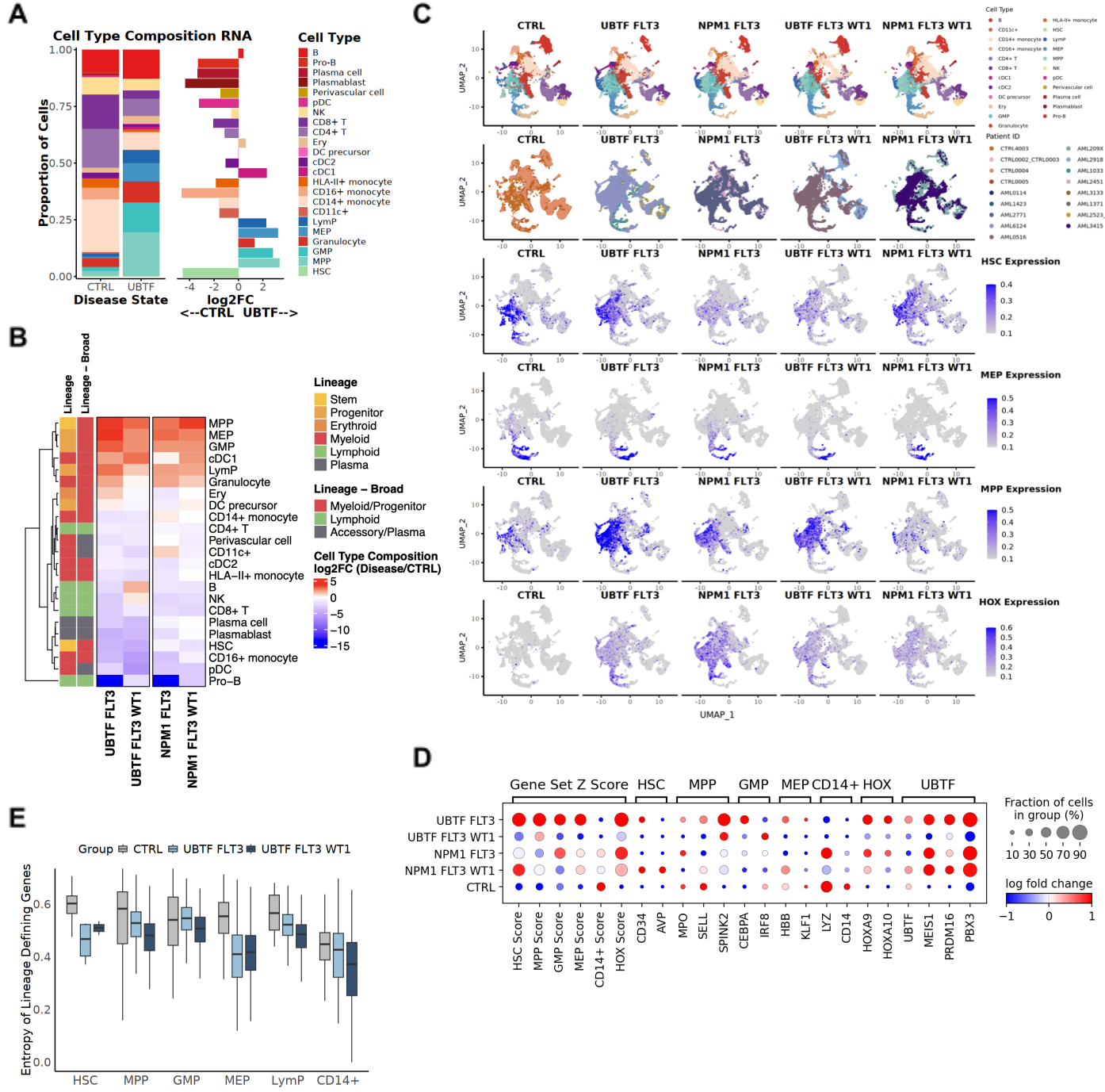


Figure 2. Transcriptional remodeling and lineage bias across *UBTF* *FLT3*-mutant AML subgroups

(A) Proportional abundance of annotated cell types in control and *UBTF*-*FLT3* samples (left) based on scRNA-seq data, with corresponding log2FC in cell type composition between the two disease states (right). (B) Heatmap showing log2FC in cell type composition across mutational subgroups relative to control groups. (C) UMAP embeddings of single-cell transcriptomes annotated by cell type, and expression of lineage-specific scores (bottom: HSC, MEP, MPP, HOX) across control and mutant groups. (D) Dot plot representing the proportion of cells expressing hematopoietic lineage scores and *UBTF*-associated transcriptional regulators (*UBTF*, *MEIS1*, *PRDM16*, *PBX3*) across mutation subgroups. Dot size reflects the fraction of cells expressing each respective gene or score, log2FC is the relative differential expression across the mutation cohorts. (E) Boxplots depict normalized entropy of lineage-defining gene expression across hematopoietic

populations in control and *UBTF*-mutant AML patients. Entropy was computed from the expression distribution of hematologic lineage signature genes to capture transcriptional heterogeneity within each cell type. Lower entropy reflects reduced lineage diversity, consistent with aberrant lineage restriction and bias toward dysregulated differentiation trajectories.

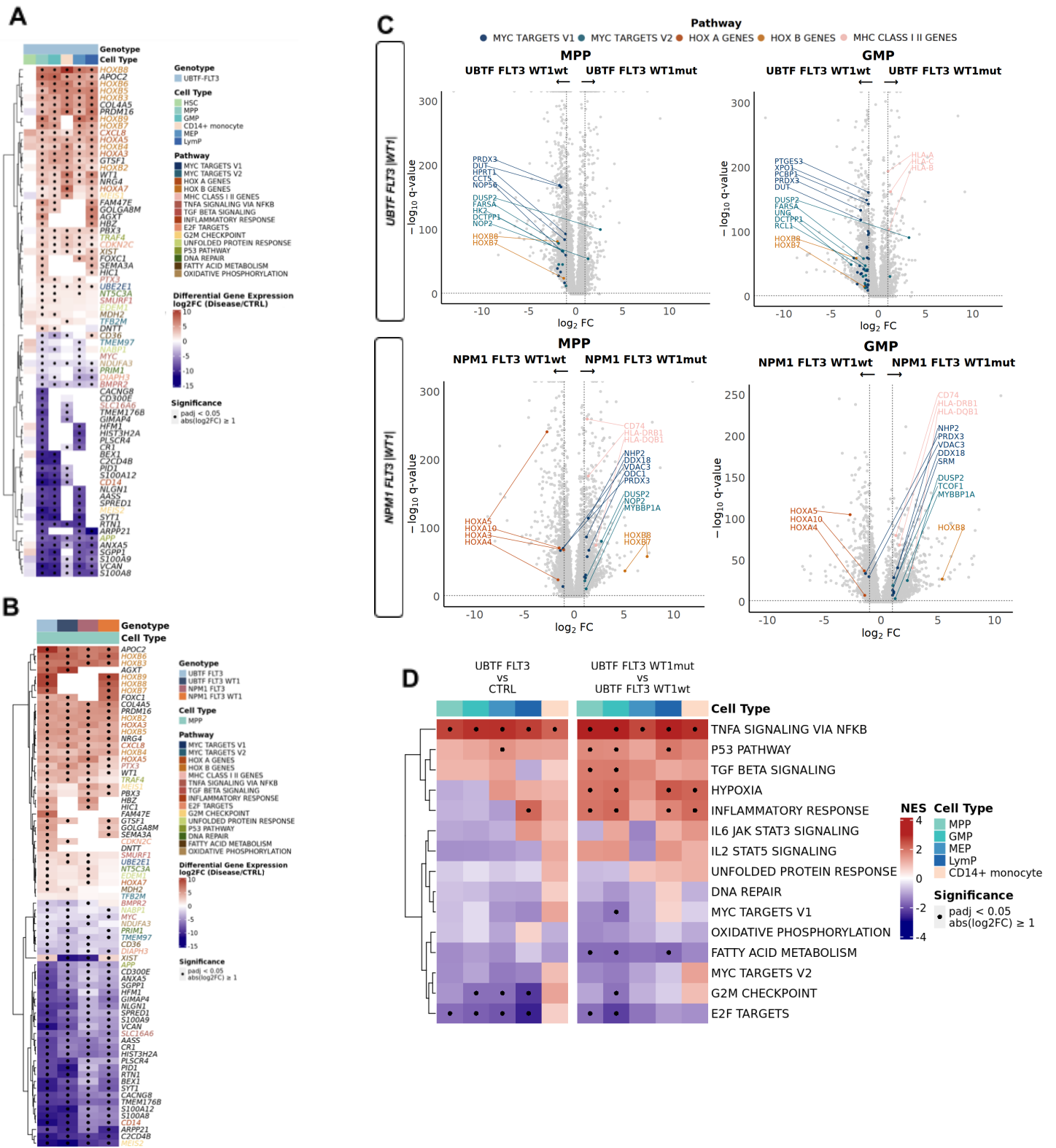


Figure 3. WT1 co-mutation in *UBTF*-*FLT3*-mutant AML drives transcriptional reprogramming and inflammatory pathway activation across myeloid lineages.

(A-B) Heatmaps of differentially expressed genes (DEGS) (log2FC relative to control) across MPP cells comparing (A) *UBTF FLT3* to CTRL and (B) *UBTF* and *NPM1* related co-mutations. Genes are annotated by associated hallmark pathways (right) and black dots indicate significant genes for each respective cell type and mutation status compared to the control. (C) Volcano plots of differential gene expression comparing *WT1* mutant versus *WT1* wild-type in *UBTF FLT3* (top) or *NPM1 FLT3* (bottom) AML in progenitor cell populations. Highlighted genes represent hallmark transcriptional programs. (D) Gene set enrichment analysis (GSEA) comparing *UBTF FLT3* and *WT1* co-mutant subtypes across progenitor and myeloid cell populations from ranked DEG analysis. Heatmaps display normalized enrichment scores (NES) for selected pathways. Black dots indicate significance. Left: effect of *UBTF FLT3* co-mutation across patients; Right: effect of *WT1* mutations in *UBTF FLT3* patients.

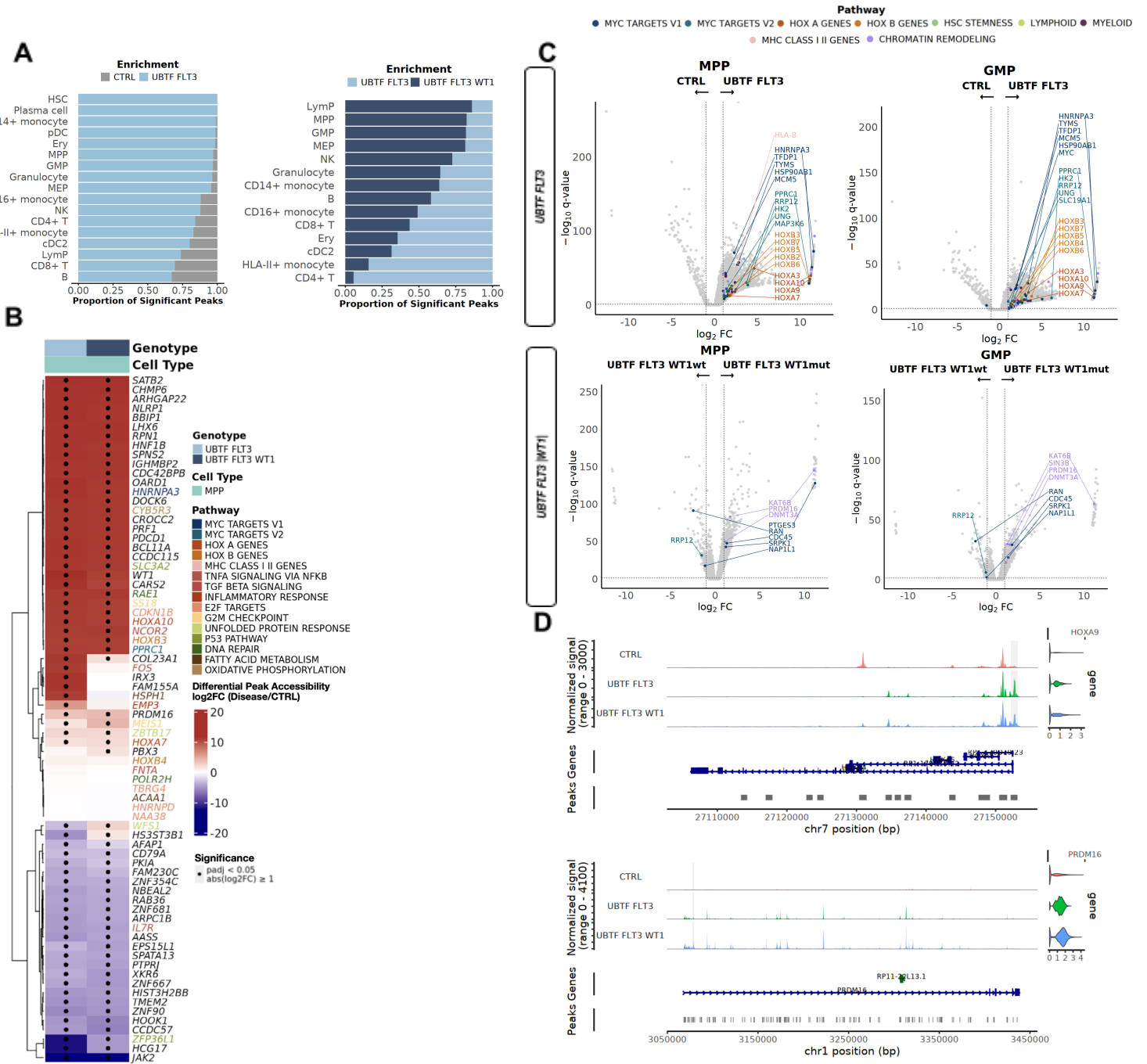


Figure 4. *UBTF-FLT3*-mutant AML rewires myeloid progenitor programs through epigenomic remodeling, though more prominently in *WT1* co-mutants

(A) Chromatin accessibility (scATAC-seq) profiling reveals cell-type specific enrichment of differentially accessible peaks in UBTF FLT3 AML compared to control (left) and in WT1 co-mutant versus WT1 wild-type UBTF FLT3 AML (right). Bar plots show the proportion of significant peaks per cell type. (B) Volcano plots of differentially expressed genes in progenitor populations across UBTF FLT3 mutations. Highlighted genes represent significant enrichment for hallmark transcriptional programs. (C) Volcano plots of (DEGS) (log2FC relative to control) across MPP cells comparing *WT1* wild-type and *WT1* mutant populations across patients harboring *UBTF* *FLT3* patients. Highlighted genes represent hallmark transcriptional programs, and black dots indicate significance. (D) Chromatin accessibility tracks at *HOXA9* and *PRDM16* loci across UBTF *FLT3* genotypes and controls, with corresponding accessibility violin plots.

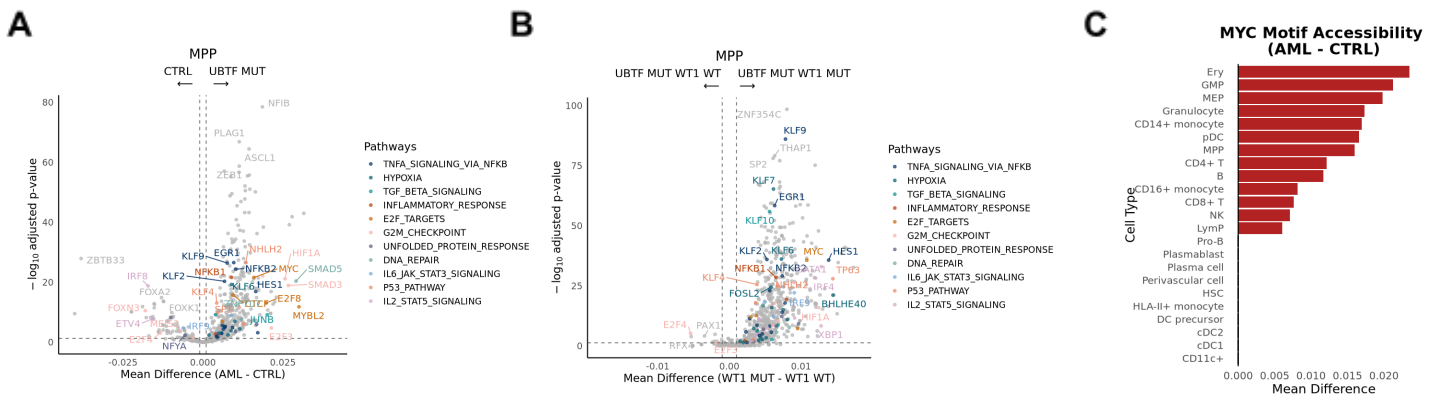


Figure 5. *UBTF-FLT3*-mutant AML is characterized by increased accessibility of MYC and inflammatory TF motifs in myeloid progenitors

(A) Differential motif accessibility in MPP cells comparing AML and control samples. (B) Differential motif accessibility in *UBTF-FLT3*-mutant MPP cells stratified by *WT1*-mutations. (C) Mean difference in MYC motif accessibility across cell types, ranked by magnitude, highlighting cell types that are susceptible to epigenetic alterations and changes in chromatin accessibility across conditions.

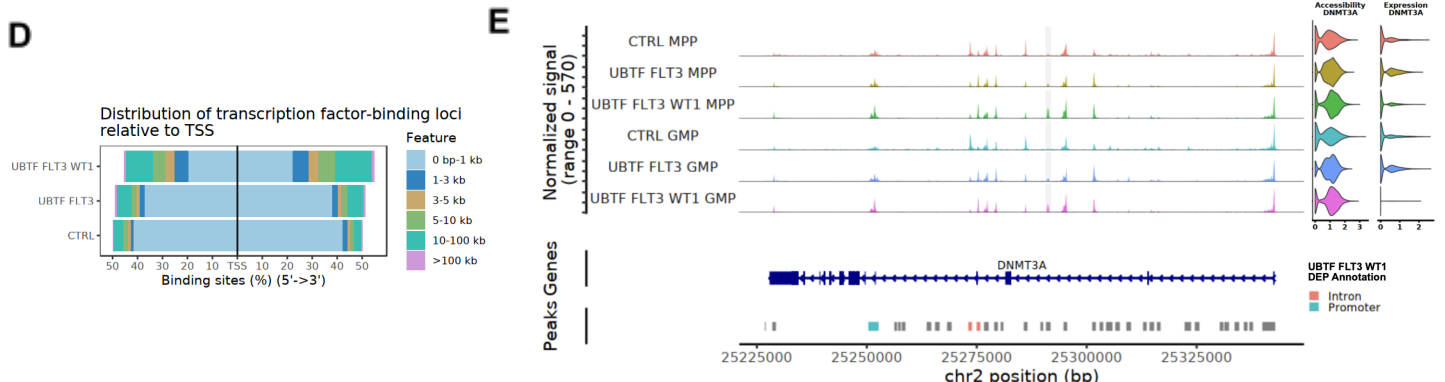
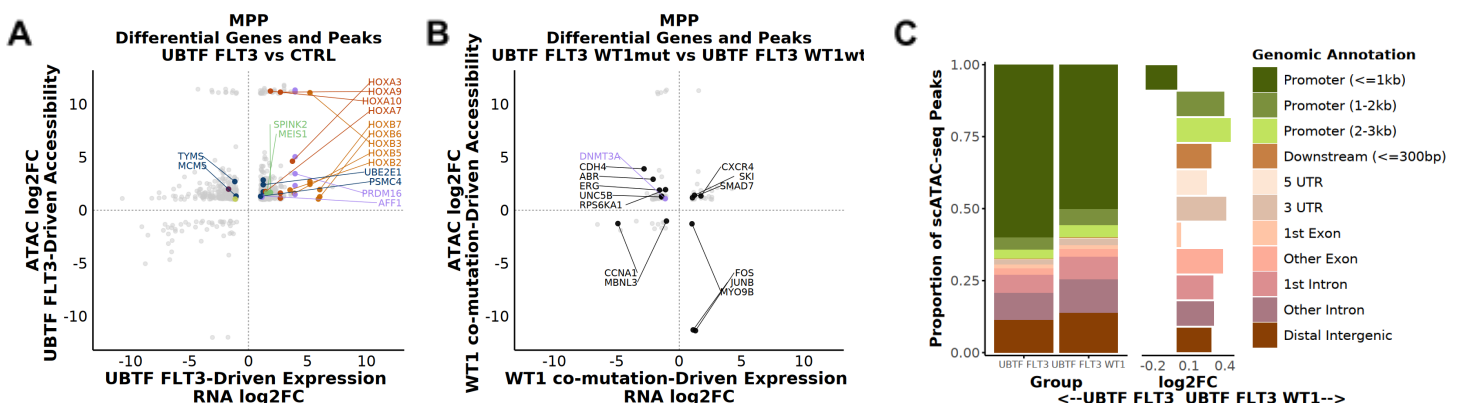


Figure 6. Coordinated transcriptional and epigenetic alterations in *UBTF*-mutant AML myeloid progenitors

(A-B) Integrated analysis of scRNA expression and chromatin accessibility (scATAC) in MPPs comparing (A) *UBTF* *FLT3*-mutant AML to healthy control and (B) *UBTF* *FLT3*-mutant stratified by *WT1* co-mutation. Genes with significant and concordant shifts in both modalities are shown, with significantly enriched hallmark associated genes highlighted. (C) Genomic distribution of differentially accessible peaks relative to *WT1* co-mutation status (left) and their genomic annotations (right). (D) Distribution of predicted transcription factor-binding loci relative to transcription start site (TSS) in differentially expressed peaks (DEPs) across genotypes. (E) Chromatin accessibility tracks at *DMNT3A* loci across *UBTF* *FLT3* genotypes and controls, with corresponding accessibility violin plots.

Experimental overview to elucidate transcriptional and mutational landscapes in AML

To systematically characterize cellular heterogeneity and mutational architecture in AML, we performed multi-omic single-cell and genomic profiling across a cohort of 21 patient samples. Our strategy integrated scRNA-seq, scATAC-seq, and WES (Figure 1A).

We first examined cell type composition across the cohort using both scRNA-seq and scATAC-seq. Stacked bar plots revealed marked shifts in the abundance of hematopoietic populations in AML relative to healthy controls (Figure 1B). AML samples exhibited a skewing toward progenitor populations such as multipotent progenitors (MPPs), granulocyte-monocyte progenitors (GMPs), and erythroid precursors, whereas control samples displayed a broader representation of differentiated lineages, including B cells, NK cells, and monocytes. These trends were consistent across both transcriptional and chromatin modalities, underscoring the robustness of our annotations and the lineage bias inherent to leukemic transformation.

To explore the genetic underpinnings of these shifts, we analyzed somatic mutations using WES. A curated panel of recurrently mutated AML genes (e.g., *UBTF*, *WT1*, *FLT3*, *NPM1*) was used to define mutation status for each patient (Figure 1B). Mutation profiles revealing the co-occurrence of *UBTF* with *WT1* or *FLT3* in a subset of AML patients. Samples with *UBTF-FLT3* and *WT1* co-mutations frequently exhibited pronounced alterations in cell type composition, including depletion of lymphoid populations (CD4+/CD8+ T cells, NK cells) and expansion of immature myeloid states (GMPs, CD14+ monocytes) consistent with their aggressive transcriptional phenotype.

Expansion of progenitor cell populations and differentiation block in *UBTF*-, *FLT3*-, and *WT1*- mutant AML subgroups

In dissecting the relationship between transcriptional states and mutational subgroups in AML, we stratified our scRNA-seq dataset by genotype and evaluated both cell type composition and lineage-specific expression programs across disease states (Figure 2A–D). We first quantified the proportional abundance of

hematopoietic cell types in control versus *UBTF* *FLT3*-mutant samples. Compared to healthy controls, *UBTF* *FLT3*-mutant samples demonstrated a marked expansion of early progenitor populations, particularly MPPs, GMPs, and megakaryocyte-erythroid progenitors (MEPs) (Figure 2A, left). In contrast, differentiated populations such as B cells, NK cells, and monocytes were depleted. Corresponding log₂ fold change (log₂FC) values confirmed a skewing toward immature progenitor states in *UBTF* *FLT3* -mutant (Figure 2A, right), consistent with a block in differentiation that underscores leukemic transformation.

Lineage bias was assessed across genetically defined AML subgroups, focusing on patients harboring *UBTF*, *FLT3*, *WT1*, and *NPM1* mutations. Hierarchical clustering of log₂ fold changes in cell type composition relative to controls revealed distinct transcriptional architectures associated with each mutational group (Figure 2B). All samples, though most prominently *UBTF* *FLT3*-mutants, displayed the strongest enrichment for MPP and MEP states, consistent with a shift toward early progenitor identity. Co-mutation with *WT1* (*UBTF* *FLT3* *WT1*) did not significantly amplify bias, in contrast to *NPM1* *FLT3*-mutants which showed more pronounced progenitor skewing with *WT1* co-mutation. This exemplified the context-dependent effect of co-mutations such as *WT1*, and the mutation-specific nature of lineage distribution in AML and point to divergent mechanisms of differentiation blockades.

UMAP embeddings were used to visualize these transcriptional shifts at single-cell resolution, annotated by cell type, patient identity, and hematopoietic lineage signature scores (Figure 2C). Undifferentiated clusters were most notably expanded in *UBTF* *FLT3*-mutant subgroups as shown by elevated expression of HSC-, MPP-, and MEP-associated gene programs, indicating increased self-renewal and priming of multiple lineages while suppressing terminal differentiation. *HOX* gene expression was strongly enriched in AML patients who did not harbor *WT1* co-mutations. This coordinated upregulation of early hematopoietic programs alongside *HOX* activation suggests a convergence on aberrant self-renewal and disrupted differentiation as a significant feature of *UBTF*-driven AML.

To evaluate transcription factor activity, the expression of *UBTF*-associated regulators (*UBTF*, *MEIS1*, *PRDM16*, *PBX3*) and hematopoietic lineage scores were quantified using dot plots (Figure 2D). The *UBTF* *FLT3*-mutant subgroup exhibited the highest expression of these regulators, along with coordinated activation of *HOX* gene programs commonly associated with leukemogenesis. A large fraction of cells expressed these

programs, reflecting a mutation-driven transcriptional reprogramming not observed in healthy controls or *NPM1* *FLT3* cases.

Transcriptional dysregulation within defined hematopoietic populations was quantified by entropy scores based on the expression of lineage-defining gene sets (Figure 2E). In healthy controls, higher entropy in progenitor and mature populations reflects normal transcriptional diversity associated with dynamic differentiation. In contrast, *UBTF*-mutant AML samples exhibited significantly lower entropy across these same populations, indicating a progressive loss of transcriptional plasticity. This suggests that while healthy hematopoiesis supports flexible lineage transitions, *UBTF*-mutant AML enforces a more homogeneous, lineage-restricted state. There overall appears to be a trend that increased mutation and co-mutation burden leads to decreased entropy, transcriptional homogeneity and lineage restriction. This effect was most pronounced in *UBTF* *FLT3* *WT1*-mutant cases, particularly within terminal myeloid compartments such as CD14+ monocytes. This supports a model in which *UBTF*-driven AML adopts a constrained, progenitor-like identity with impaired differentiation capacity.

These findings demonstrate that *UBTF* mutations drive a robust stem-like transcriptional state characterized by impaired differentiation and sustained progenitor identity. *UBTF*-*FLT3* mutant AMLs converge on a transcriptional bottleneck marked by early myeloid progenitor expansion, HOX-driven self-renewal, and failure to execute terminal differentiation. Rather than multilineage priming, this state reflects arrested myeloid-biased stemness, modulated by *WT1* co-mutation and divergent from *NPM1* *FLT3*-mutants. This transcriptional signature is distinct from other mutational backgrounds and may contribute to the aggressive clinical phenotype observed in *UBTF*-mutant AML.

WT1 co-mutation amplifies inflammatory programs in *UBTF*-mutant AML

To elucidate how *WT1* co-mutation alters the transcriptional landscape in *UBTF*-mutant AML, differential gene expression and GSEA were performed across key myeloid lineages, comparing *WT1*-wild-type and *WT1*-mutant backgrounds within the *UBTF*-mutant and *NPM1*-mutant contexts (Figure 3).

UBTF *FLT3*-mutant AML demonstrated striking overexpression of *HOXA* and *HOXB* family genes, consistent with a transcriptional program promoting self-renewal and impaired differentiation (Figure 3A). Additional upregulated genes included *PRDM16*, *CDK2*, and *GTF2H1*, supporting roles in chromatin regulation

and cell cycle progression (Figure 3A). In contrast, genes involved in interferon response, cell adhesion, and myeloid maturation (*S100A8*, *S100A12*, *CSCL2*, *ANK3*) were markedly down regulated across compartments, indicating a suppression of immune and differentiation programs (Figure 3A). These trends were conserved across all myeloid lineages, highlighting a shared core of *UBTF FLT3*-driven transcriptional dysregulation (Figure 3A, Figure 1E). GSEA of these ranked DEGs support these trends, as *UBTF FLT3* mutants had significant enrichment for MYC targets, inflammatory response, TNF α signaling via NF- κ B and apoptosis - findings that align with a stem-like, stress-resistant leukemic state (Figure 3D). Additionally, G2M checkpoint and E2F target pathways were enriched in controls, emphasizing that *UBTF FLT3*-mutant AML bypass normal cell cycle regulation through alternative mechanisms (Figure 3D).

To define how *WT1* co-mutation modules transcriptional programs within AML subtypes, we additionally performed DGE across progenitor cell types, stratifying *UBTF FLT3* and *NPM1 FLT3* mutant AML samples by *WT1* status (Figure 3B). *WT1*-mutant AML cases, both *UBTF FLT3* and *NPM1 FLT3*, exhibited marked upregulation of *HOX* cluster genes, key chromatin regulators (*PRDM16*, *TET2*) and inflammatory mediators (*TRAF4*, *TNFRSF1B*) (Figure 3B). Apoptotic genes (*BAX*, *CASP6*), metabolic regulators (*NDUF* family) and myeloid maturation genes (*S100A8*, *S100A12*) were significantly downregulated, suggesting suppression of terminal differentiation and stress response checkpoints (Figure 3B). In directly comparing the effect of *WT1* co-mutation across *UBTF FLT3* and *NPM1 FLT3* populations, *WT1*-mutant MPPs exhibited significant repression of MYC target genes and upregulation of *HOX B* family genes, a trend that is similarly observed in GMPs (Figure 3C). This indicates that *WT1* co-mutation in *UBTF FLT3* populations shifts leukemic progenitors toward an inflammatory, hypoxic state in early progenitors. This likely contributes to a clonally dominant, stress-tolerant leukemic state, which would ultimately lead to chemoresistance and immune escape in *UBTF FLT3* driven AML.

Collectively, these data demonstrate that *WT1* mutations in the context of *UBTF FLT3*-mutant AML drive a convergence on inflammatory and apoptotic signaling across MPP, GMP, and monocytic compartments. This genotype-specific transcriptional reprogramming may enhance leukemic cell fitness under inflammatory conditions and promote immune evasion or resistance to differentiation therapy.

A cooperative epigenetic and transcriptional rewiring mechanism underlies *UBTF*-driven leukemogenesis

To assess whether transcriptional reprogramming in *UBTF* *FLT3*-mutant AML is accompanied by epigenetic changes in chromatin structure, scATAC-seq was performed on bone marrow cells from *UBTF* *FLT3* and *UBTF* *FLT3 WT1* mutated AML and control samples (Figure 4).

To explore the global impact of *UBTF* *FLT3 WT1* co-mutation status on chromatin accessibility, we quantified the proportion of significantly altered peaks across hematopoietic cell types using scATAC-seq. *UBTF* *FLT3* AML displayed widespread chromatin remodeling, with significantly increased peak accessibility across early progenitor compartments (Figure 4A, left). Incorporation of *WT1* co-mutation further amplified this effect (Figure 4B, right). *WT1*-mutant *UBTF* *FLT3* AML samples showed the highest proportion of differential peaks in progenitor populations, further reinforcing lineage bias effects (Figure 4A, right).

We further dissected how *WT1* co-mutation reprograms in *UBTF* *FLT3* patients, where indifferent to the presence of *WT1* *UBTF* *FLT3* showed significant chromatin remodeling (Figure 4B). Highly accessible regions were enriched near *HOX* gene clusters, chromatin regulators (*PRDM16*, *CDK6*, *ZBTB17*), consistent with epigenetic activation of self-renewal and developmental programs. Conversely, reduced accessibility was observed near genes associated with differentiation and immune response, including *JAK2*, *ZFP36L1*, and *HCG17*. These findings are consistent with activation of self-renewal programs, and silencing of myeloid differentiation factors as shown in our scRNA-seq (Figure 4B).

Compared to controls, progenitor populations had increased accessibility of *MYC* and *HOX* related pathways (Figure 4C, top), though this was not statistically significant when stratified by *WT1* co-mutations (Figure 4C, bottom). *WT1* co-mutation was instead marked by cooperative remodeling of chromatin architecture at epigenetic regulators (Figure 4C, bottom), suggesting that *UBTF* *FLT3* is a primary driver of *HOX/MYC*-linked chromatin accessibility, while *WT1* co-mutation more prominently affects epigenetic plasticity.

In identifying gene regulatory elements associated with disease-specific enhancer activation, chromatin accessibility tracks were visualized at key leukemogenic loci. *UBTF*-mutant samples displayed focal enhancer accessibility at the *HOXA9* and *PRDM16* loci, suggesting direct epigenetic priming of oncogenic programs (Figure 4D). These enhancer elements were largely inaccessible in control samples, underscoring AML-specific chromatin remodeling.

To further characterize transcription factor (TF) activity underlying this chromatin rewiring, differential motif accessibility analysis was performed. In MPPs, motif accessibility was significantly increased at sites recognized by inflammatory and apoptotic regulators, including NF- κ B, E2F, and SMAD3, in *UBTF*-mutant samples compared to controls (Figure 5A). Stratification by *WT1* status revealed further upregulation of MYC, CEBP, and KLF motif accessibility in *WT1*-mutant *UBTF* cells (Figure 5B), implicating these TFs in the cooperative remodeling of leukemic chromatin.

Analysis of mean MYC motif accessibility across all cell types revealed that myeloid progenitors (GMP, MPP, MEP) exhibited the greatest increases in chromatin accessibility at MYC motifs in AML compared to controls (Figure 5C). This cell type–specific motif enrichment suggests that *UBTF*-mutant AML cells are particularly dependent on MYC-driven transcriptional programs at the epigenetic level.

An integrated analysis of scRNA-seq and scATAC-seq profiles in MPPs from *UBTF* *FLT3*-mutant stratified by *WT1* co-mutation and healthy controls further enables the identification of genes exhibiting concerted regulation at transcriptional and epigenetic levels (Figure 6). Genes in the upper right quadrant were strongly enriched for *HOXA* and *HOXB* clusters, suggesting that *UBTF* *FLT3* mutations activate a core self-renewal program through coordinated epigenetic and transcriptional mechanisms (Figure 6A). In contrast, a small subset of genes including *TYMI* and *MCM5* displayed increased accessibility but reduced expression (upper left quadrant), potentially reflecting bivalent chromatin states or post-transcriptional suppression (Figure 6A). In comparison, *WT1* co-mutation appears to enhance the accessibility though reduce the expression of chromatin remodeling genes (*DNMT3A*, *ERG*, *CDH4*, and *RPS6KA1*), reinforcing the role of *WT1* in promoting developmental plasticity and enhancer priming for future activation (Figure 6B). *WT1* co-mutation also leads to the decreased accessibility though increased expression of genes related to stress response (*FOS*, *JUNB*), implying that *WT1* co-mutation enforces for the suppression of immune response though these genes are ultimately activated by non-canonical enhancers (Figure 6B). Together, this suggests that *WT1* co-mutation selectively remodels the chromatin landscape, introducing epigenetic flexibility that may contribute to clonal expansion.

We additionally annotated differentially accessible peaks by their genomic features to further gain insight to alterations of genomic architecture in response to *WT1* co-mutations (Figure 6C). Across both *WT1*

groups, the majority of accessible peaks mapped to promoter regions and close to the TSS, consistent with canonical gene regulation. However, *WT1*-mutant samples exhibited a relative depletion of promoter-proximal peaks and a corresponding increase in accessibility at distal intergenic and intronic regions (Figure 6C). This shift suggests that *WT1* co-mutation drives enhancer-centric chromatin remodeling, potentially activating non-canonical regulatory elements, further suggesting that *WT1* co-mutations enhance epigenetic plasticity by opening chromatin outside of promoter regions and enables flexible transcriptional responses through alternative enhancers (Figure 6C, Figure 6B).

WT1 co-mutation further shifts transcription factor binding away from TSS-proximal regions (Figure 6D). In control samples, TF binding sites were concentrated within 1 kb of the TSS, reflecting canonical promoter-driven regulation. In contrast, *UBTF FLT3* AML samples showed a broader distribution of binding sites, including increased motif enrichment at regions 3-10 and 10-100 kb from the TSS, a redistribution that was even more pronounced in *WT1* co-mutant AML (Figure 6D). This trend in *WT1* co-mutants is consistent with hallmarks of distal enhancer engagement by long-range chromatin remodeling (Figure 6C) and a shift in regulatory architecture from promoter-centric to enhancer-driven transcriptional plasticity, allowing leukemic progenitors to activate pathways outside conventional promoter regulation (Figure 6C, Figure 6D).

We visualized chromatin accessibility at the *DNMT3A* locus across progenitor populations to access epigenetic regulation effects of *WT1* co-mutation (Figure 6B, Figure 6E). Compared to healthy controls and *UBTF FLT3*-mutants, *WT1*-mutants exhibited increased accessibility and though decreased expression of *DNMT3A* compared to *UBTF FLT3*, further allowing for transcriptional plasticity and leukemic adaption (Figure 6B, Figure 6E).

These findings support a model in which *UBTF FLT3* mutations initiate broad epigenomic remodeling that primes leukemic progenitors for oncogenic transcriptional programs. Co-mutation with *WT1* further amplifies chromatin accessibility at regulatory elements associated with inflammatory and self-renewal signatures, suggesting a cooperative mechanism of leukemogenesis through integrated epigenetic and transcriptional rewiring.

DISCUSSION

AML is characterized by profound cellular and genetic heterogeneity, driven by complex mutational interactions that perturb hematopoietic differentiation and fuel malignant self-renewal. In this study, we integrate single-cell transcriptomic, chromatin accessibility, and whole-exome sequencing data across AML patient samples to delineate the cooperative impact of *UBTF*, *FLT3*, and *WT1* mutations on leukemic cell identity and potential prognosis for these patients. Our multi-modal approach reveals a convergence on early progenitor expansion, and enhancer-centric epigenetic remodeling as central features of *UBTF*-driven AML, which are further modulated by *WT1* co-mutation.

Our findings uncover that *UBTF-FLT3* mutant AMLs exhibit a marked skewing toward multipotent and erythroid-myeloid progenitor states, a pattern that aligns with their transcriptional upregulation of *HOX* gene clusters and self-renewal factors such as *MEIS1*, *PRDM16*, and *PBX3*. These programs are known drivers of leukemic stemness in other AML subtypes, including *KMT2A*-rearranged and *NPM1*-mutant AML^{26,38,42-44} and their enrichment here points to a shared transcriptional architecture.

By integrating scATAC-seq, we further show that *UBTF-FLT3* mutations drive widespread chromatin remodeling in early progenitors, with preferential opening of enhancer regions near *HOXA/B* loci and *MYC* targets. This suggests that *UBTF*-driven AMLs do not merely transcribe stemness programs—they epigenetically prime progenitor cells for them. This enhancer activation mirrors patterns described in other aggressive leukemias such as *NPM1*-mutant AMLs, where leukemogenesis is similarly tied to the epigenetic dysregulation of distal regulatory elements.⁴⁵

WT1 co-mutation emerges as a critical modulator of these effects. While prior studies have identified *WT1* as a bifunctional regulator acting either as an oncogene or tumor suppressor depending on context,²¹⁻²⁵ our data show that in *UBTF-FLT3*-mutant AML, *WT1* promotes inflammatory transcriptional programs while amplifying chromatin accessibility at distal regulatory elements. This shift is associated with reduced promoter-proximal TF binding and increased enhancer-centric activity, pointing to a model where *WT1* co-mutation introduces epigenetic plasticity that enables adaptation under stress or immune pressure. Such plasticity likely contributes to immune evasion, therapeutic resistance, and clonal dominance, consistent with outcomes observed in *WT1*-mutant AML.^{16-19, 26}

Our entropy-based quantification of transcriptional diversity provides insight into the functional consequences of mutation burden. *UBTF*- and *WT1*-mutant AML samples showed progressively reduced transcriptional entropy within defined progenitor compartments, indicating a narrowed differentiation potential. This finding resonates with the concept of lineage entrapment seen in therapy-resistant AML clones,^{27,46} and supports a model in which combinatorial mutation burden enforces a rigid progenitor-like state that is both resilient and poorly responsive to differentiation cues.

Together, these data establish *UBTF* *FLT3* *WT1*- mutant AML as a distinct molecular subtype with a core signature of *HOX/MYC*-driven self-renewal, epigenetic enhancer remodeling, and immune suppression. Our findings suggest that this leukemic state is maintained through both transcriptional and chromatin-level reprogramming, offering potential targets for therapy. Menin inhibitors, which block *HOX/MEIS1*-driven transcription, have shown efficacy in KMT2A- and *NPM1*-mutant AML³⁸ and may prove effective in *UBTF-TD* AML given the shared dependency on *HOX* programs. Similarly, targeting chromatin remodelers or immune-evasive signatures associated with *WT1* co-mutation may represent potential combination strategies.

Future studies should focus on functional validation of candidate enhancers and regulatory circuits identified here, as well as on the therapeutic vulnerabilities introduced by the epigenetic rigidity and inflammatory reprogramming of *WT1*-mutant AML. Our integrative framework provides insights for dissecting complex mutational interactions in leukemia and may aid in the development of personalized therapeutic strategies tailored to mutation-specific regulatory architectures.

METHODS

PATIENT SAMPLE PREPARATION

Whole exome sequencing (WES)

Genomic DNA was extracted from mononuclear cells isolated from bone marrow aspirates or peripheral blood using the QIAamp DNA Mini Kit (Qiagen) following the manufacturer's protocol. DNA quality and quantity were assessed using a NanoDrop spectrophotometer and Qubit fluorometer. Exome libraries were prepared using the Agilent SureSelect Human All Exon V7 kit, according to the manufacturer's protocol. Library quality was verified using an Agilent Bioanalyzer. Pooled libraries were sequenced on an Illumina NovaSeq 6000 platform with 2×150 bp paired-end reads, targeting a median coverage of >100× for tumor samples.

scRNA-seq and scATAC-seq

Fresh bone marrow and peripheral blood mononuclear cells were washed with 0.04% BSA/PBS, filtered through a 40 µm strainer, and assessed for viability (>85%) using Trypan Blue. For scRNA-seq, cells were processed using the 10x Genomics Chromium Single Cell 3' Kit v3.1, targeting 10,000 cells per reaction. For scATAC-seq, nuclei were isolated by lysis in ice-cold buffer (10 mM Tris-HCl pH 7.4, 10 mM NaCl, 3 mM MgCl₂, 0.1% Tween-20, 0.1% NP-40, 0.01% Digitonin), washed, filtered, and counted before loading. Transposition and barcoding were performed using the 10x Genomics Single Cell ATAC Kit v1.1, also targeting 10,000 nuclei. All libraries were prepared according to manufacturer protocols and sequenced on an Illumina NovaSeq 6000 (2×150 bp for scRNA-seq; 2×50 bp for scATAC-seq).

COMPUTATIONAL ANALYSIS

Whole exome sequencing (WES)

Somatic variant calling

Whole exome sequencing (WES) was performed on DNA extracted from bone marrow or peripheral blood mononuclear cells. Library preparation was carried out using the Agilent SureSelect Human All Exon V7 kit, followed by paired-end sequencing (2×150 bp) on an Illumina NovaSeq 6000 platform, targeting a median coverage of 100× in tumor samples and 50× in matched normals where available.

Raw sequencing reads were trimmed for quality and adapter content using Trimmomatic v0.39, then aligned to the GRCh38 human reference genome using BWA-MEM v0.7.17. PCR duplicates were marked with Picard, and base quality recalibration was performed with GATK v4.2.0.0.

Somatic variants were identified using Mutect2 (GATK) in paired or tumor-only mode. Variants were annotated with Ensembl VEP v104, and filtered to retain nonsynonymous single-nucleotide variants (SNVs), frameshift and nonframeshift indels, and splice region variants with variant allele frequency (VAF) ≥5% and read depth ≥10×.

Recurrently mutated genes in AML (e.g., *UBTF*, *FLT3*, *WT1*, *NPM1*) were curated for downstream analyses.

scRNA-seq data quality control and preprocessing

Single-cell RNA sequencing data were processed using a standardized pipeline for alignment, quantification, and quality control. Raw FASTQ files were demultiplexed and aligned to the human reference genome (GRCh38, Ensembl build 93) using the Cell Ranger (v6.1.2) pipeline (10x Genomics). Alignment of reads was performed via the STAR aligner within Cell Ranger, and gene-level quantification was conducted to generate a cell-by-gene expression matrix, incorporating both unique molecular identifiers (UMIs) and cell-specific barcodes. This process resulted in a feature-barcode matrix containing transcript counts for each individual cell.

The feature-barcode matrix was subsequently imported into R (v4.3.3) and analyzed using the Seurat (v5.0.1) package. Initial quality control (QC) steps included filtering cells based on the number of detected genes, total UMI counts, and the percentage of reads mapping to mitochondrial genes. Specifically, cells with fewer than 500 detected genes, more than 7,500 genes (to remove potential doublets), or >15% mitochondrial gene content were excluded.

Following QC, normalization was performed using SCTransform, which models UMI counts using a regularized negative binomial model while regressing out sources of unwanted variation, including mitochondrial gene content and total UMI counts per cell. When analyzing multiple samples or experimental conditions, dataset integration was conducted using Seurat's reciprocal PCA-based anchor finding workflow. This enabled batch correction across samples while preserving shared biological variance.

Dimensionality reduction was achieved via Principal Component Analysis (PCA) using highly variable genes identified during normalization. The top principal components were used to construct a k-nearest neighbors (KNN) graph, followed by graph-based clustering using the Louvain algorithm. Clustering resolution was tuned based on dataset complexity and visualized using Uniform Manifold Approximation and Projection (UMAP).

For cell type annotation, differential gene expression analysis was performed using FindMarkers in Seurat, which applies the MAST (Model-based Analysis of Single-cell Transcriptomics) framework to account for zero-inflation in scRNA-seq data. Cluster-specific marker genes were manually curated and matched against established hematopoietic gene signatures for lineage classification.

The resulting annotated Seurat object was used for downstream analyses, including differential expression, pathway enrichment, and integration with scATAC-seq data.

scRNA-seq data analysis

Data visualization

Two-dimensional embeddings were generated using Seurat (v5.0.1). After dimensionality reduction with Principal Component Analysis (PCA), a shared nearest neighbor (SNN) graph was constructed using the top 30 principal components. Uniform Manifold Approximation and Projection (UMAP) was used to visualize cellular relationships in a low-dimensional space, with parameters tuned based on dataset complexity (e.g., dims = 1:30, min.dist = 0.3, n.neighbors = 30). All UMAP plots, violin plots, dot plots, and heatmaps were produced using Seurat, ggplot2 (v3.4.4), and ComplexHeatmap (v2.16.0) in R.

Gene signature scores

Gene signature scores were computed using the AddModuleScore function in Seurat (v5.0.1). For each predefined gene set, this function calculates the average expression across genes in the set for each cell, subtracted by the aggregated expression of randomly selected control gene sets matched for average expression levels. This approach mitigates gene set size and expression bias. To further reduce the impact of baseline expression variability across signatures, all scores were calculated using z-scored, SCTransform-normalized expression data. Resulting module scores were used to quantify transcriptional programs related to stemness, cell cycle, inflammation, and lineage-specific differentiation across annotated cell populations.

Differential gene expression analysis - Seurat

Differential gene expression analysis was performed using the Wilcoxon rank-sum test as implemented in the FindMarkers and FindAllMarkers functions in Seurat (v5.0.1). Comparisons were conducted between healthy control and AML cells, stratified by mutational status and annotated cell type. The analysis was performed on SCTransform-normalized expression values using the Pearson residuals from the negative binomial regression model. All detected genes were included without prior restriction to predefined gene sets.

\log_2 fold changes were calculated for each gene between specified groups, and genes were ranked based on both statistical significance and effect size. Adjusted p-values were calculated using Bonferroni correction to control for multiple hypothesis testing. The top differentially expressed genes were selected for downstream visualization, including volcano plots, dot plots, and heatmaps.

Differential gene expression analysis - Scanpy

For additional DEG visualizations (dotplot across multiple groups) functions of Scanpy were implemented. Differential gene expression analysis across multiple groups was performed using the Wilcoxon rank-sum test, as implemented in `scanpy.tl.rank_genes_groups` (Scanpy v1.9.1). Comparisons were conducted between healthy controls and AML cells, stratified by their mutation status. The analysis was based on the log-normalized gene expression matrix, and all detected genes were included without prior gene set restriction. \log_2 fold changes were computed relative to each gene's expression across the specified groups. Genes were ranked by statistical significance and effect size (log-fold change), and the top differentially expressed genes were selected for downstream visualization. Adjusted p-values were calculated using the Bonferroni correction to control for multiple hypothesis testing.

scATAC-seq data quality control and preprocessing

scATAC-seq data were processed using an integrated pipeline for fragment alignment, quality control (QC), dimensionality reduction, and cell type annotation within the Seurat framework. Raw BCL files were demultiplexed using `cellranger-atac mkfastq`, and aligned to the human reference genome (GRCh38, Ensembl build 93) using Cell Ranger ATAC (v2.1.0) (10x Genomics), generating fragment files containing barcode-tagged chromatin accessibility reads.

Fragment files were imported into R (v4.3.3) and analyzed using Signac (v1.13.0) and Seurat (v5.0.1). Cells were filtered based on standard scATAC-seq quality control metrics, including total fragment counts, transcription start site (TSS) enrichment, and nucleosome signal. Cells with >3,000 and <50,000 fragments, TSS enrichment >2, and nucleosome signal <4 were retained. Cells with a low fraction of fragments in peaks were removed to ensure robust chromatin signal.

A gene activity matrix was computed by aggregating chromatin accessibility within gene bodies and promoter regions using the GeneActivity() function in Signac. This matrix was log-normalized and used for dimensionality reduction alongside peak accessibility data.

Dimensionality reduction was performed using Latent Semantic Indexing (LSI) on a term frequency-inverse document frequency (TF-IDF) normalized peak-cell matrix. The first 2 components were excluded to minimize technical noise, and the remaining components were used to construct a shared nearest neighbor (SNN) graph for clustering. UMAP was used to visualize the resulting low-dimensional embedding.

Cell type annotation of scATAC-seq data was conducted by transferring cell labels from the matched scRNA-seq dataset. Specifically, RNA and ATAC modalities were integrated using FindTransferAnchors() and TransferData() in Seurat, leveraging the gene activity matrix as the ATAC expression input. Following preprocessing, individual patient-level Seurat objects were merged into a single dataset for downstream analysis.

scATAC-seq data analysis

Visualization and downstream analysis of scATAC-seq data followed workflows analogous to those described above for scRNA-seq.

GSEA

Gene set enrichment analysis was performed using clusterProfiler (v4.8.1) in R, applied to ranked gene lists generated from differential expression results computed with Seurat's FindMarkers function. Genes were ranked by average \log_2 fold change between specified groups (e.g., *UBTF*-mutant vs control) without applying significance thresholds. Enrichment analysis was conducted against the MSigDB Hallmark gene sets as well as manually curated cell type-specific gene signatures derived from prior studies. The GSEA function was run with 10,000 permutations and default parameters. Enrichment results were filtered using an adjusted p-value threshold of 0.05 (Bonferroni correction).

Statistical Analysis

Pairwise comparisons gene expression across mutation groups (Figure 4D) were calculated by Mann-Whitney U, and p-values were adjusted for multiple testing using the bonferroni correction ($q < 0.05$).

REFERENCES

1. Tenen, D.G. (2003). Disruption of differentiation in human cancer: AML shows the way. *Nat Rev Cancer* 3, 89–101. <https://doi.org/10.1038/nrc989>.
2. Klco, J.M., Spencer, D.H., Miller, C.A., Griffith, M., Lamprecht, T.L., O’Laughlin, M., Fronick, C., Magrini, V., Demeter, R.T., Fulton, R.S., et al. (2014). Functional Heterogeneity of Genetically Defined Subclones in Acute Myeloid Leukemia. *Cancer Cell* 25, 379–392. <https://doi.org/10.1016/j.ccr.2014.01.031>. 1.
3. Miles, L.A., Bowman, R.L., Merlinsky, T.R., Csete, I.S., Ooi, A.T., Durruthy-Durruthy, R., Bowman, M., Famulare, C., Patel, M.A., Mendez, P., et al. (2020). Single-cell mutation analysis of clonal evolution in myeloid malignancies. *Nature* 587, 477–482. <https://doi.org/10.1038/s41586-020-2864-x>.
4. Umeda, M., Ma, J., Huang, B.J., Hagiwara, K., Westover, T., Abdelhamed, S., Barajas, J.M., Thomas, M.E., Walsh, M.P., Song, G., et al. (2022). Integrated Genomic Analysis Identifies *UBTF* Tandem Duplications as a Recurrent Lesion in Pediatric Acute Myeloid Leukemia. *Blood Cancer Discovery* 3, 194–207. <https://doi.org/10.1158/2643-3230.BCD-21-0160>.
5. DiNardo, C.D., Erba, H.P., Freeman, S.D., and Wei, A.H. (2023). Acute myeloid leukaemia. *The Lancet* 401, 2073–2086. [https://doi.org/10.1016/S0140-6736\(23\)00108-3](https://doi.org/10.1016/S0140-6736(23)00108-3).
6. Makkar, H., Majhi, R.K., Goel, H., Gupta, A.K., Chopra, A., Tanwar, P., and Seth, R. Acute myeloid leukemia: novel mutations and their clinical implications.
7. Tamamyan, G., Kadia, T., Ravandi, F., Borthakur, G., Cortes, J., Jabbour, E., Daver, N., Ohanian, M., Kantarjian, H., and Konopleva, M. (2017). Frontline treatment of acute myeloid leukemia in adults. *Critical Reviews in Oncology/Hematology* 110, 20–34. <https://doi.org/10.1016/j.critrevonc.2016.12.004>.
8. Molica, M., Breccia, M., Foa, R., Jabbour, E., and Kadia, T.M. (2019). Maintenance therapy in AML: The past, the present and the future. *American J Hematol* 94, 1254–1265. <https://doi.org/10.1002/ajh.25620>.

9. Bolouri, H., Farrar, J.E., Triche, T., Ries, R.E., Lim, E.L., Alonzo, T.A., Ma, Y., Moore, R., Mungall, A.J., Marra, M.A., et al. (2018). The molecular landscape of pediatric acute myeloid leukemia reveals recurrent structural alterations and age-specific mutational interactions. *Nat Med* 24, 103–112.
<https://doi.org/10.1038/nm.4439>.
10. Takahashi, S. (2011). Current findings for recurring mutations in acute myeloid leukemia. *J Hematol Oncol* 4, 36. <https://doi.org/10.1186/1756-8722-4-36>.
11. Martelli, M.P., Sportoletti, P., Tiacci, E., Martelli, M.F., and Falini, B. (2013). Mutational landscape of AML with normal cytogenetics: Biological and clinical implications. *Blood Reviews* 27, 13–22.
<https://doi.org/10.1016/j.blre.2012.11.001>.
12. Rubnitz, J.E., Gibson, B., and Smith, F.O. (2010). Acute Myeloid Leukemia. *Hematology/Oncology Clinics of North America* 24, 35–63. <https://doi.org/10.1016/j.hoc.2009.11.008>.
13. Shih AH, Abdel-Wahab O, Patel JP and Levine RL. The role of mutations in epigenetic regulators in myeloid malignancies. *Nat Rev Cancer* 2012; 12: 599-612.
14. Yang, L., Rau, R., and Goodell, M.A. (2015). DNMT3A in haematological malignancies. *Nat Rev Cancer* 15, 152–165. <https://doi.org/10.1038/nrc3895>.
15. Othman, J., Potter, N., Ivey, A., Tazi, Y., Papaemmanuil, E., Jovanovic, J., Freeman, S.D., Gilkes, A., Gale, R., Rapoz-D'Silva, T., et al. (2024). Molecular, clinical, and therapeutic determinants of outcome in *NPM1* -mutated AML. *Blood* 144, 714–728. <https://doi.org/10.1182/blood.2024024310>.
16. Awada, H., Durmaz, A., Gurnari, C., Kishtagari, A., Zawit, M., Pagliuca, S., and Visconte, V. (2021). Friend or foe? The case of Wilms' Tumor 1 (WT1) mutations in acute myeloid leukemia. *Blood Cells, Molecules, and Diseases* 88, 102549. <https://doi.org/10.1016/j.bcmd.2021.102549>.
17. Pronier, E., Bowman, R.L., Ahn, J., Glass, J., Kandoth, C., Merlinsky, T.R., Whitfield, J.T., Durham, B.H., Gruet, A., Hanasoge Somasundara, A.V., et al. (2018). Genetic and epigenetic evolution as a contributor to WT1-mutant leukemogenesis. *Blood* 132, 1265–1278.
<https://doi.org/10.1182/blood-2018-03-837468>.

18. Atluri, H., DiGennaro, J., Patel, K.P., Routbort, M., Oran, B., Issa, G.C., Short, N.J., Daver, N., Kadia, T.M., Ravandi, F., et al. (2023). Clinical and Prognostic Implications of *WT1* Mutations in De Novo and Relapsed Acute Myeloid Leukemia. *Blood* *142*, 959–959. <https://doi.org/10.1182/blood-2023-188319>.
19. Wang, T., Hua, H., Wang, Z., Wang, B., Cao, L., Qin, W., Wu, P., Cai, X., Chao, H., and Lu, X. (2022). Frequency and clinical impact of *WT1* mutations in the context of *CEBPA*-mutated acute myeloid leukemia. *Hematology* *27*, 994–1002. <https://doi.org/10.1080/16078454.2022.2103964>.
20. Rampal, R., and Figueroa, M.E. (2016). Wilms tumor 1 mutations in the pathogenesis of acute myeloid leukemia. *Haematologica* *101*, 672–679. <https://doi.org/10.3324/haematol.2015.141796>.
21. Yang, L., Han, Y., Saurez Saiz, F., and Minden, M.D. (2007). A tumor suppressor and oncogene: the *WT1* story. *Leukemia* *21*, 868–876. <https://doi.org/10.1038/sj.leu.2404624>.
22. Becker, H., Marcucci, G., Maharry, K., Radmacher, M.D., Mrózek, K., Margeson, D., Whitman, S.P., Paschka, P., Holland, K.B., Schwind, S., et al. (2010). Mutations of the Wilms tumor 1 gene (*WT1*) in older patients with primary cytogenetically normal acute myeloid leukemia: a Cancer and Leukemia Group B study. *Blood* *116*, 788–792. <https://doi.org/10.1182/blood-2010-01-262543>.
23. Hou, H.-A., Huang, T.-C., Lin, L.-I., Liu, C.-Y., Chen, C.-Y., Chou, W.-C., Tang, J.-L., Tseng, M.-H., Huang, C.-F., Chiang, Y.-C., et al. (2010). *WT1* mutation in 470 adult patients with acute myeloid leukemia: stability during disease evolution and implication of its incorporation into a survival scoring system. *Blood* *115*, 5222–5231. <https://doi.org/10.1182/blood-2009-12-259390>.
24. Herzer, U., Crocoll, A., Barton, D., Howells, N., and Englert, C. (1999). The Wilms tumor suppressor gene *wt1* is required for development of the spleen. *Current Biology* *9*, 837-S1. [https://doi.org/10.1016/S0960-9822\(99\)80369-8](https://doi.org/10.1016/S0960-9822(99)80369-8).
25. Ellisen LW, Carlesso N, Cheng T, Scadden DT, Haber DA. The Wilms tumor suppressor *WT1* directs stage-specific quiescence and differentiation of human hematopoietic progenitor cells. *EMBO J.* 2001;20(8):1897-1909.
26. El Hussein, S., DiNardo, C.D., Takahashi, K., Khouri, J.D., Fang, H., Furudate, K., Lyapichev, K.A., Garces, S., Kanagal-Shamanna, R., Ok, C.Y., et al. (2022). Acquired *WT1* mutations contribute to

- relapse of NPM1-mutated acute myeloid leukemia following allogeneic hematopoietic stem cell transplant. *Bone Marrow Transplant* 57, 370–376. <https://doi.org/10.1038/s41409-021-01538-w>.
27. Duployez, N., Vasseur, L., Kim, R., Largeaud, L., Passet, M., L'Haridon, A., Lemaire, P., Fenwarth, L., Geffroy, S., Helevaut, N., et al. (2023). UBTF tandem duplications define a distinct subtype of adult de novo acute myeloid leukemia. *Leukemia* 37, 1245–1253. <https://doi.org/10.1038/s41375-023-01906-z>.
28. Kwon, H., and Green, M.R. (1994). The RNA polymerase I transcription factor, upstream binding factor, interacts directly with the TATA box-binding protein. *Journal of Biological Chemistry* 269, 30140–30146. [https://doi.org/10.1016/S0021-9258\(18\)43788-X](https://doi.org/10.1016/S0021-9258(18)43788-X).
29. Yang, L., Rau, R., and Goodell, M.A. (2015). DNMT3A in haematological malignancies. *Nat Rev Cancer* 15, 152–165. <https://doi.org/10.1038/nrc3895>.
30. Sanij, E., Diesch, J., Lesmana, A., Poortinga, G., Hein, N., Lidgerwood, G., Cameron, D.P., Ellul, J., Goodall, G.J., Wong, L.H., et al. (2015). A novel role for the Pol I transcription factor UBTF in maintaining genome stability through the regulation of highly transcribed Pol II genes. *Genome Res.* 25, 201–212. <https://doi.org/10.1101/gr.176115.114>.
31. Stefanovsky, V.Y., and Moss, T. (2008). The splice variants of UBF differentially regulate RNA polymerase I transcription elongation in response to ERK phosphorylation. *Nucleic Acids Research* 36, 5093–5101. <https://doi.org/10.1093/nar/gkn484>.
32. Štros, M., Launholt, D., and Grasser, K.D. (2007). The HMG-box: a versatile protein domain occurring in a wide variety of DNA-binding proteins. *Cell. Mol. Life Sci.* 64, 2590–2606. <https://doi.org/10.1007/s00018-007-7162-3>.
33. Edvardson, S., Nicolae, C.M., Agrawal, P.B., Mignot, C., Payne, K., Prasad, A.N., Prasad, C., Sadler, L., Nava, C., Mullen, T.E., et al. (2017). Heterozygous De Novo UBTF Gain-of-Function Variant Is Associated with Neurodegeneration in Childhood. *The American Journal of Human Genetics* 101, 267–273. <https://doi.org/10.1016/j.ajhg.2017.07.002>.
34. Zhang, J., Zhang, J., Liu, W., Ge, R., Gao, T., Tian, Q., Mu, X., Zhao, L., and Li, X. (2021). UBTF facilitates melanoma progression via modulating MEK1/2-ERK1/2 signalling pathways by promoting GIT1 transcription. *Cancer Cell Int* 21, 543. <https://doi.org/10.1186/s12935-021-02237-8>.

35. Xie, Z., Tang, R., Gao, X., Xie, Q., Lin, J., Chen, G., and Li, Z. (2018). A meta-analysis and bioinformatics exploration of the diagnostic value and molecular mechanism of miR-193a-5p in lung cancer. *Oncol Lett.* <https://doi.org/10.3892/ol.2018.9174>.
36. Tsoi, H., Lam, K.C., Dong, Y., Zhang, X., Lee, C.K., Zhang, J., Ng, S.C., Ng, S.S.M., Zheng, S., Chen, Y., et al. (2017). Pre-45s rRNA promotes colon cancer and is associated with poor survival of CRC patients. *Oncogene* 36, 6109–6118. <https://doi.org/10.1038/onc.2017.86>.
37. Barros-Silva, J.D., Paulo, P., Bakken, A.C., Cerveira, N., Løvf, M., Henrique, R., Jerônimo, C., Lothe, R.A., Skotheim, R.I., and Teixeira, M.R. (2013). Novel 5' Fusion Partners of ETV1 and ETV4 in Prostate Cancer. *Neoplasia* 15, 720-IN6. <https://doi.org/10.1593/neo.13232>.
38. Barajas, J.M., Rasouli, M., Umeda, M., Hiltenbrand, R., Abdelhamed, S., Mohnani, R., Arthur, B., Westover, T., Thomas, M.E., Ashtiani, M., et al. (2024). Acute myeloid leukemias with *UBTF* tandem duplications are sensitive to menin inhibitors. *Blood* 143, 619–630.
<https://doi.org/10.1182/blood.2023021359>.
39. Kaburagi, T., Shiba, N., Yamato, G., Yoshida, K., Tabuchi, K., Ohki, K., Ishikita, E., Hara, Y., Shiraishi, Y., Kawasaki, H., et al. (2023). *UBTF* -INTERNAL tandem duplication as a novel poor prognostic factor in pediatric acute myeloid leukemia. *Genes Chromosomes & Cancer* 62, 202–209.
<https://doi.org/10.1002/gcc.23110>.
40. Stratmann, S., Yones, S.A., Mayrhofer, M., Norgren, N., Skaftason, A., Sun, J., Smolinska, K., Komorowski, J., Herlin, M.K., Sundström, C., et al. (2021). Genomic characterization of relapsed acute myeloid leukemia reveals novel putative therapeutic targets. *Blood Advances* 5, 900–912.
<https://doi.org/10.1182/bloodadvances.2020003709>.
41. Umeda, M., Ma, J., Westover, T., Ni, Y., Song, G., Maciaszek, J.L., Rusch, M., Rahbarinia, D., Foy, S., Huang, B.J., et al. (2024). A new genomic framework to categorize pediatric acute myeloid leukemia. *Nat Genet* 56, 281–293. <https://doi.org/10.1038/s41588-023-01640-3>.
42. Heikamp, E.B., Henrich, J.A., Perner, F., Wong, E.M., Hatton, C., Wen, Y., Barwe, S.P., Gopalakrishnapillai, A., Xu, H., Uckelmann, H.J., et al. (2022). The menin-MLL1 interaction is a

- molecular dependency in *NUP98*-rearranged AML. *Blood* **139**, 894–906.
<https://doi.org/10.1182/blood.2021012806>.
43. Grembecka, J., He, S., Shi, A., Purohit, T., Muntean, A.G., Sorenson, R.J., Showalter, H.D., Murai, M.J., Belcher, A.M., Hartley, T., et al. (2012). Menin-MLL inhibitors reverse oncogenic activity of MLL fusion proteins in leukemia. *Nat Chem Biol* **8**, 277–284. <https://doi.org/10.1038/nchembio.773>.
44. Klossowski, S., Miao, H., Kempinska, K., Wu, T., Purohit, T., Kim, E., Linhares, B.M., Chen, D., Jih, G., Perkey, E., et al. (2020). Menin inhibitor MI-3454 induces remission in MLL1-rearranged and NPM1-mutated models of leukemia. *Journal of Clinical Investigation* **130**, 981–997.
<https://doi.org/10.1172/JCI129126>.
45. Cao, Z., Shu, Y., Wang, J., Wang, C., Feng, T., Yang, L., Shao, J., and Zou, L. (2022). Super enhancers: Pathogenic roles and potential therapeutic targets for acute myeloid leukemia (AML). *Genes & Diseases* **9**, 1466–1477. <https://doi.org/10.1016/j.gendis.2022.01.006>.
46. Van Galen, P., Hovestadt, V., Wadsworth Ii, M.H., Hughes, T.K., Griffin, G.K., Battaglia, S., Verga, J.A., Stephansky, J., Pastika, T.J., Lombardi Story, J., et al. (2019). Single-Cell RNA-Seq Reveals AML Hierarchies Relevant to Disease Progression and Immunity. *Cell* **176**, 1265–1281.e24.
<https://doi.org/10.1016/j.cell.2019.01.031>.